Scaling of Fock-space propagator and multifractality across the many-body localization transition

Jagannath Sutradhar^{1,*}, Soumi Ghosh^{1,2,*}, Sthitadhi Roy^{2,3,4},

David E. Logan^{3,5}, Subroto Mukerjee¹, Sumilan Banerjee^{1*}

¹ Centre for Condensed Matter Theory, Department of Physics, Indian Institute of Science, Bangalore 560012, India

² International Centre for Theoretical Sciences, Tata Institute of Fundamental Research, Bengaluru 560089, India

³ Physical and Theoretical Chemistry, Oxford University, South Parks Road, Oxford OX1 3QZ, United Kingdom

⁴ Rudolf Peierls Centre for Theoretical Physics, Clarendon Laboratory,

Oxford University, Parks Road, Oxford OX1 3PU, United Kingdom

⁵ Department of Physics, Indian Institute of Science, Bangalore 560012, India[†]

(Dated: March 16, 2022)

We implement a recursive Green function method to extract the Fock space (FS) propagator and associated self-energy across the many-body localization (MBL) transition, for one-dimensional interacting fermions in a random onsite potential. We show that the typical value of the imaginary part of the local FS self-energy, Δ_t , related to the decay rate of an initially localized state, acts as a probabilistic order parameter for the thermal to MBL phase transition; and can be used to characterize critical properties of the transition as well as the multifractal nature of MBL states as a function of disorder strength W. In particular, we show that a fractal dimension D_s extracted from Δ_t jumps discontinuously across the transition, from $D_s < 1$ in the MBL phase to $D_s = 1$ in the thermal phase. Moreover, Δ_t follows an asymmetrical finite-size scaling form across the thermal-MBL transition, where a non-ergodic volume in the thermal phase diverges with a Kosterlitz-Thouless like essential singularity at the critical point W_c , and controls the continuous vanishing of Δ_t as W_c is approached. In contrast, a correlation length (ξ) extracted from Δ_t exhibits a power-law divergence on approaching W_c from the MBL phase.

A many-body localized (MBL) phase is a fascinating non-equilibrium state of matter which can originate in isolated quantum systems in the presence of disorder and interactions [1–4]. In the MBL phase, high-energy eigenstates violate the Eigenstate Thermalization Hypothesis (ETH) [5–7], and local memory can be retained up to arbitrarily long times under time evolution. After the early landmark papers [8, 9], a mathematical proof [10] and numerous numerical studies [11–16] have provided strong evidence in favour of the existence of the MBL phase in one dimension. However, the universal properties of the transition from the thermal or ETH phase to the MBL phase remain under active debate [17–23]. This is mainly due to the challenge to "first principles" numerical verification of theoretical scenarios, posed by the exponentially growing Fock-space dimension (\mathcal{N}_F) with system size L [11, 13, 17, 24, 25]. To complement calculations on microscopic models, several phenomenological renormalisation group-based approaches have been employed [18, 26–28], which suggest a Kosterlitz-Thouless (KT)-like scenario for the MBL transition.

A further complementary approach to MBL is to consider it as an effective 'Fock-space (FS) localization' problem of a fictitious particle on the complex, correlated FS graph (or 'lattice') [16, 29–31]. This has led to crucial insights such as the role of strong FS correlations in stabilising the MBL phase [30–33], multifractality of eigenstates therein [17, 34–37] and, importantly, a numerical scaling theory of the MBL transition in terms of FS inverse participation ratios (IPR) of eigenstates, which is consistent with a KT-like scenario [35, 36]. Here we ask the question: can a scaling theory of the MBL transition

be formulated in terms of FS propagators?

In this work we answer this question in the affirmative, by studying the propagator or Green function on the FS lattice for a fermionic chain with $L \leq 22$. In particular, we extract the local Feenberg self-energy [30, 38, 39] from the diagonal elements of the FS propagator. As known since Anderson's seminal paper [40], the typical value of the imaginary part of the Feenberg self-energy, Δ_t , acts as a probabilistic order parameter in the thermodynamic limit for Anderson transitions [40–43]. This quantity has recently been employed to construct a selfconsistent mean-field theory of the MBL transition on the Fock space [30, 31]. However, numerically exact evaluation of the FS self-energy for the microscopic models of MBL, and analysis of their behaviour across the MBL transition, is scarce. Here we fill this void and show that the MBL transition from ergodic extended states in the thermal phase to multifractal states in the MBL phase [17, 34–37], is manifest in an anomalous scaling of Δ_t with the Fock-space dimension. This, together with a scaling theory of the MBL transition based on the order parameter Δ_t , that is consistent with the KT-like scenario, constitutes the central result of the work.

The FS propagator contains information about the ergodic/non-ergodic nature of the phase, as different eigenstates contribute to it, based on their energy and amplitudes over FS lattice sites. From a technical point of view, computation of the propagator in principle requires all eigenstates. This restricts the system sizes accessible to numerical exact diagonlization (ED), which for L > 18 can access only a limited number of eigenstates [44]. To access larger sizes, comparable to

those accessible via parallelised shift-invert method [44] or POLFED [45], but at significantly cheaper computational cost, we compute the FS propagators using a standard recursive Green function method [46–48], but adapted to the FS graph. Moreover, for the reasons discussed below, we study a scaled version of the self-energy, viz. Δ_t/\sqrt{L} , and refer to it as Δ_t throughout the rest of the paper for notational convenience. Employing the recursive method, we obtain the following main results:

1. The typical value Δ_t of the self-energy is finite in the thermal phase. It vanishes $\propto \mathcal{N}_F^{-(1-D_s)}$ in the MBL phase and at the critical point, where $D_s < 1$ is a fractal dimension reflecting the multifractal nature of the states. D_s changes discontinuously across the MBL transition, from $D_s < 1$ to $D_s = 1$ throughout the thermal phase. 2. The finite-size scaling of Δ_t as a function of disorder strength (W) is consistent with an asymmetric finite-size scaling form [35, 36, 49, 50] across the MBL transition. Scaling on the thermal side is controlled by a non-ergodic volume scale Λ , which diverges with an essential singularity $\Lambda \sim \exp(b/\sqrt{\delta W})$, $[\delta W = (W_c - W), b \sim \mathcal{O}(1)]$ at a critical disorder (W_c) , redolent of a KT-like transition. Scaling on the MBL side by contrast is controlled by a FS correlation length (ξ) , which exhibits a power-law divergence on approaching criticality. Moreover, the scaling theory implies that in the thermodynamic limit Δ_t vanishes continuously on approaching the transition from the thermal side as $\sim \exp\left[-b'/\sqrt{\delta W}\right]$ with $b' \sim \mathcal{O}(1)$.

As already mentioned, multifractal characterization of MBL states [17, 34] and numerical scaling theory consistent with a KT-like MBL transition have been obtained via study of eigenstate IPRs [35, 36]. However our work reveals for the first time the multifractality and KT-type critical scaling in terms of a FS order parameter for the thermal-MBL transition.

Model.— We study the following standard model [11–13, 15–17, 51] of MBL for a fermionic chain with an i.i.d. random onsite potential $\epsilon_i \in [-W, W]$ of strength W on $i = 1, \ldots, L$ sites and nearest-neighbour repulsion (V),

$$\mathcal{H} = t \sum_{i=1}^{L-1} \left(c_i^{\dagger} c_{i+1} + c_{i+1}^{\dagger} c_i \right) + \sum_{i=1}^{L} \epsilon_i \hat{n}_i + V \sum_{i=1}^{L-1} \hat{n}_i \hat{n}_{i+1}. \tag{1}$$

Here c_i^{\dagger} (c_i) is the fermion creation (annihilation) operator for site i, with number operator $\hat{n}_i = c_i^{\dagger} c_i$. We choose t = 0.5 and V = 1 to be consistent with earlier studies; and study the model in the half-filled sector at 'infinite temperature', which corresponds to the middle of the many-body energy spectrum. In this case, the model shows a thermal to MBL transition at a critical disorder $W_c \simeq 3.7 - 4.2$ [17].

To describe the many-body system in Fock space, we employ the occupation-number basis $\{|I\rangle\}$ of particles on the real-space sites, $|I\rangle=|n_1^{(I)}n_2^{(I)}..n_L^{(I)}\rangle$ with $n_i^{(I)}\in 0$ or 1. In this basis, the Hamiltonian Eq. (1) takes the form

of a tight-binding model [30, 33, 52]

$$\mathcal{H} = \sum_{I,J} T_{IJ} |I\rangle \langle J| + \sum_{I} \mathcal{E}_{I} |I\rangle \langle I|, \qquad (2)$$

but on the FS lattice [Fig. 1(a)]. Here, the FS "hopping" $T_{IJ} = t$ when $|I\rangle$ and $|J\rangle$ are connected by a single nearest-neighbor hop in real-space, and $T_{IJ} = 0$ otherwise. The onsite "disorder" potential at FS site I is $\mathcal{E}_I = \sum_i \epsilon_i n_i^{(I)} + V \sum_i n_i^{(I)} n_{i+1}^{(I)}$, and is a combination of the real-space disorder potential and the nearest-neighbor interaction.

The disorder-averaged many-body density of states for the model is a Gaussian as a function of energy E, with the mean $\propto L$ and variance $\mu_E^2 = (t^2 + W^2/6 + V^2/8)L/2$ [52]. As a result, to treat different system sizes on the same footing and for the theory to have a well-defined thermodynamic limit [31], we scale the parameters and work with a rescaled $\tilde{\mathcal{H}} = \mathcal{H}/\sqrt{L}$ [30, 31, 52]. This leads directly to the scaled version of the self-energy mentioned above. We also set the mean many-body energy to zero, by transforming $\tilde{\mathcal{H}}$ to $\tilde{\mathcal{H}} - 1$ Tr $\tilde{\mathcal{H}}/\mathcal{N}_F$ for each disorder realization, since the middle of the spectrum fluctuates with disorder realization for a finite system.

Recursive Green's function method.— Elements of the retarded FS propagator $G(E) = [(E + i\eta)\mathbb{1} - \tilde{\mathcal{H}}]^{-1}$ are computed by implementing the standard recursive method [46–48, 53] at the middle (E = 0) of the energy spectrum. We choose the broadening (or regulator) $\eta(W) = \sqrt{2\pi}\mu_E/(\sqrt{L}\mathcal{N}_F)$ [30, 52], the mean many-body level spacing of $\tilde{\mathcal{H}}$, which depends on disorder strength W through the variance μ_E^2 . We arrange the Fock space basis states in a layered lattice structure, as illustrated in Fig. 1(a). Crucially, this is local, in that sites belonging to any slice or layer are connected through hopping only to sites belonging to the nearest-neighbor layers. It is this locality that allows for an efficient implementation of the method for the FS lattice, as detailed in Supplementary Material (SM), Sec. S1.

We calculate the diagonal elements $G_{II}(E) = \langle I|G(E)|I\rangle$, where $I \in$ the middle slice M [Fig. 1(a)]. As mentioned in the introduction, we extract one of the quintessential characterizations of the localization properties, the imaginary part Δ_I of the Feenberg self-energy $\Sigma_I(E) = X_I(E) - i\Delta_I(E) \equiv G_{II}^{-1}(E) - (E + i\eta - \mathcal{E}_I)$. We consider the distributions of Δ_I , in particular the disorder-averaged typical value $\Delta_t(E)$ given by $\ln \Delta_t = \langle \ln \Delta_I \rangle_{I,\{\epsilon_i\}}$, where $\langle ... \rangle_{I,\{\epsilon_i\}}$ denotes averaging over $I \in M$ and disorder configurations $\{\epsilon_i\}$. Depending on L, ~ 150 to 10,000 disorder realizations are employed to generate the distribution of Δ_I (SM, Sec. S1).

Multifractality and scaling theory from the imaginary part of Feenberg self-energy.— The imaginary part $\Delta_I(E)$ of the self-energy determines the energy-resolved decay time $[\Delta_I(E)^{-1}]$ of a localized initial state $|I\rangle$ or, alternatively, the life time of an excitation with energy E created at the FS lattice site I [40]. As such,

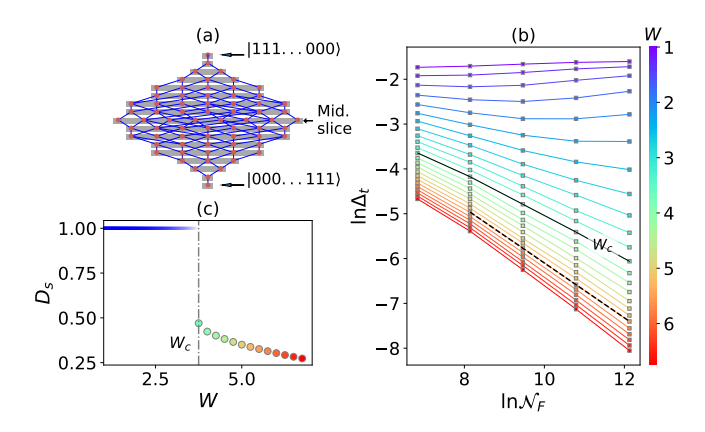


FIG. 1. (a) Fock-space lattice constructed out of real-space occupation-number basis states (orange circles), illustrated for L=8, starting at the top with $|111..000\rangle$, i.e. all particles on the left side, and ending at the bottom with all particles on the right. The hoppings (blue lines) and the slices (grey lines) are indicated. (b) $\ln \Delta_t$ as a function of $\ln \mathcal{N}_F \propto L$ for different W (color bar) across the MBL transition (W_c). The exponential decrease of Δ_t with L for $W>W_c$ is shown by the dashed grey line (linear fit) for one value of W. (c) The fractal dimension D_s obtained from the finite-size scaling theory jumps discontinuously across the transition, from $D_s < 1$ in the MBL phase to $D_s = 1$ in the thermal phase. At $W=W_c$ (vertical dash-dotted line) $D_s \simeq 0.5$.

 $\Delta_I(E)$ directly encodes information about localization or lack thereof. In the thermal phase, the typical value $\Delta_t \sim \mathcal{O}(1)$, as the initial state decays in a finite time, whereas in the MBL phase, $\Delta_t \to 0$ in the thermodynamic limit $\mathcal{N}_F \to \infty$.

Numerical results for Δ_t as a function of \mathcal{N}_F are shown in Fig. 1(b). Δ_t indeed decreases as a function of W from an $\mathcal{O}(1)$ value in the thermal phase to a value which in the MBL phase vanishes exponentially rapidly with L. Deep in the thermal phase at weak disorder, Δ_t is independent of \mathcal{N}_F . By contrast, in the MBL phase $(W > W_c)$, Δ_t decays as a power-law, $\propto \mathcal{N}_F^{-(1-D_s)}$ with $0 < D_s < 1$. As discussed later, D_s is a spectral fractal dimension which characterizes the multifractality of the MBL states. It depends on W as shown in Fig. 1(c), where D_s has been obtained from the finite-size scaling analysis discussed below. Note that at intermediate disorder in the ETH phase, Δ_t initially decays with \mathcal{N}_F for small L, before showing an increasing trend, presumably towards its finite asymptotic value in the thermodynamic limit [Fig. 1(b)]. This indicates that the systems are in the critical regime at intermediate disorder.

The bare data itself conforms to the expectation that in the thermodynamic limit Δ_t vanishes in the MBL phase and approaches a finite $\mathcal{O}(1)$ value in the thermal phase. But to analyze compellingly the critical properties of Δ_t , we perform a scaling collapse of the data using the fol-

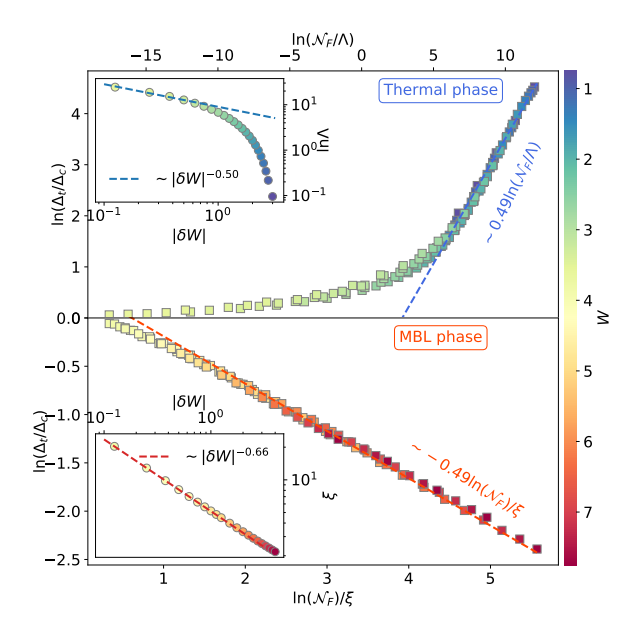


FIG. 2. Finite-size scaling collapse of $\ln(\Delta_t/\Delta_c)$ using respectively the volumic and linear scaling [Eq. (3)] in the thermal (upper panel) and MBL (lower panel) phase, with $W_c=3.75$. Upper panel: The asymptotic scaling of $\ln(\Delta_t/\Delta_c)\sim0.5\ln(\mathcal{N}_F/\Lambda)$ deep in the thermal phase is determined by the exponent $(1-D_c)\simeq0.5$ at $W=W_c$, where $\Delta_c\sim\mathcal{N}_F^{-(1-D_c)}$. Inset shows the KT-like essential singularity of the nonergodic volume, $\Lambda\sim\exp(b/\sqrt{\delta W})$ with $\delta W=(W_c-W)$, near W_c . Lower panel: Deep in the MBL phase, asymptotic scaling gives $\ln(\Delta_t/\Delta_c)\propto(\ln\mathcal{N}_F)/\xi$. The inset shows the divergence of the correlation length, $\xi\sim|\delta W|^{-\beta}$ with $\beta\simeq0.7$, on approaching the transition from the MBL phase. System sizes from L=12-22 were used to obtain the scaling.

lowing finite-size scaling ansatz [35, 36, 49],

$$\ln \frac{\Delta_t}{\Delta_c} = \begin{cases} \mathcal{F}_{\text{vol}} \left(\frac{\mathcal{N}_F}{\Lambda} \right) & : W < W_c \\ \mathcal{F}_{\text{lin}} \left(\frac{\ln \mathcal{N}_F}{\xi} \right) & : W > W_c, \end{cases}$$
(3)

where $\Delta_c = \Delta_t(W=W_c) \sim \mathcal{N}_F^{-(1-D_c)}$. The scaling ansatz states that in the ETH phase, Δ_t follows a 'volumic' scaling form where the finite-size scaling is controlled by a Fock-space volume scale, Λ [35, 36, 49]. In the MBL phase, on the other hand, the scaling form is 'linear' with the scaling controlled by a Fock-space lengthscale, ξ [35, 36, 49]. Taking $W_c = 3.75$, the good collapse of the data shown in Fig. 2 suggests that the above scaling forms are appropriate. As shown in SM Sec. S3, varying W_c between $\sim 3.5-4$ leads to comparably good scaling.

The 'non-ergodic' volume $\Lambda(W)$ [49] extracted from the scaling collapse of $\ln(\Delta_t/\Delta_c)$ in the thermal phase $(W < W_c)$ is shown in the upper panel of Fig. 2 (inset). Λ diverges at the critical point with a KT-like essential singularity, $\Lambda \sim \exp\left[b/(\delta W)^{\alpha}\right]$ with $\alpha \simeq 0.5$, where $\delta W = (W_c - W)$ and $b \sim \mathcal{O}(1)$. This kind of KT-type singularity has been predicted by a phenomenological RG

theory [18, 26–28], albeit based on a real-space picture. Throughout the ETH phase, since the eigenstates are understood to be ergodic [35], we expect $\Delta_t \sim \mathcal{O}(1)$ asymptotically in the limit $\mathcal{N}_F \gg \Lambda$. This implies for the volumic scaling function in Eq. (3) that $\mathcal{F}_{\text{vol}}(x) \sim (1-D_c) \ln x$ for $x \gg 1$. As evinced in the upper panel of Fig. 2, this is indeed the asymptotic form of the scaling function, $\mathcal{F}_{\text{vol}}(x) \sim 0.49 \ln x$ (see SM, Sec. S3 for details) from which we estimate $D_c \simeq 0.51$. This is an excellent agreement with $D_c \simeq 0.5$ obtained by fitting the raw data of Δ_t against \mathcal{N}_F for $W_c=3.75$ [Fig. 1(b)]. A significant conclusion from this is that $D_s = 1$ throughout the ETH phase and jumps discontinuously to a value $D_s < 1$ at the MBL transition, whereafter it decreases smoothly with increasing W [Fig. 1(c)]. This is in complete consonance with the discontinuity across the MBL transition of the fractal dimension characterising the Fock-space IPRs of the eigenstates [35, 36]. Furthermore, the form of the divergence of Λ and the asymptotic form of \mathcal{F}_{vol} implies that in the thermodynamic limit, Δ_t vanishes continuously as the transition is approached from the ETH side as $\Delta_t \sim \Lambda^{-(1-D_c)} \sim \exp[-b(1-D_c)/\delta W^{\alpha}]$.

In the MBL phase for $W>W_c$, the scaling collapse yields a diverging correlation length, $\xi\sim (W-W_c)^{-\beta}$ with $\beta\simeq 0.7$, as shown in the lower panel of Fig. 2 (inset). For $x=(\ln \mathcal{N}_F)/\xi\gg 1$, the asymptotic scaling is $\mathcal{F}_{\mathrm{lin}}(x)\sim -(1-D_c)x$ (SM, Sec. S3), as indeed seen in Fig. 2 lower panel. From the form of $\mathcal{F}_{\mathrm{lin}}(x)$, $\xi=(1-D_c)/(D_c-D_s)$, which implies a divergent ξ as $D_s\to D_c$, i.e. $W\to W_c+$ (SM, Sec. S3). Note that $D_c<1$ implies that the MBL critical point is actually a part of the MBL phase itself. This is consistent with the understanding that the entire MBL phase is critical in the sense that it is multifractal, and the MBL transition can be understood as the terminal end point of the line of fixed points.

Having established the critical scaling of the FS order parameter Δ_t and the volume (length) scale in the thermal (MBL) phase, we now discuss how the system-size scaling $\Delta_t \sim \mathcal{N}_F^{-(1-D_s)}$ in Fig. 1(b),(c) for $W > W_c$ is related to multifractality in the MBL phase. MBL eigenstates are known to be multifractal in nature [17, 34–37], i.e. non-ergodic but extended over $\sim \mathcal{N}_F^D$ (0 < D < 1) FS sites. Similar to the case of the local density of states discussed in Ref. [54], the multifractality can be deduced from the dependence of the typical value and the distribution of Δ_I , on the broadening parameter η for large but finite \mathcal{N}_F . In this limit, Δ_t saturates as a function of η below an energy scale $\eta_c \sim \mathcal{N}_F^{-z}$ (0 < z < 1), namely, $\Delta_t \sim \eta_c^{\theta} \sim \mathcal{N}_F^{-(1-D_s)}$ for $\eta \ll \eta_c$, whereas $\Delta_t \sim \eta^{\theta}$ for $\eta \gg \eta_c$. Here the exponent $\theta > 0$ and the spectral fractal dimension $D_s = 1 - z\theta$ lies between 0 and 1 [54]. Physically, η_c signifies the presence of an energy scale much larger than the mean level spacing \mathcal{N}_F^{-1} for multifractal states for any finite system. In our calculations, $\eta \propto \mathcal{N}_F^{-1} \ll \eta_c$, thus we expect $\Delta_t \sim \mathcal{N}_F^{-(1-D_s)}$. This is indeed the behaviour for $\Delta_t(\mathcal{N}_F)$ that we find in Fig. 1(b)

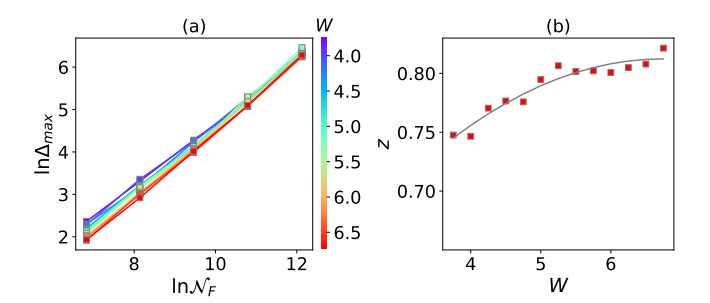


FIG. 3. (a) In the MBL phase, the scaling of Δ_{\max} with the Fock space dimension \mathcal{N}_F is shown to follow a power-law $\Delta_{\max} \propto \mathcal{N}_F^z$ for different disorder strengths (colorbar). To obtain good statistics, $\ln \Delta_{\max}$ plotted here is averaged over a few of the largest values of $\ln \Delta$ for a given L and W. (b) The exponent z, obtained from $\Delta_{\max} \sim \eta_c^{-1} \sim \mathcal{N}_F^z$ in (a), is shown to be < 1 in the MBL phase, consistent with the multifractal scaling of the self-energies. The solid line is merely a guide to the eye.

over the entire MBL range $(W>W_c)$. It is also completely consistent with the asymptotic form of the scaling function [Fig. 2 (lower panel)] and the D_s extracted from it [Fig. 1(b)]. The spectral dimension D_s can be shown to be the same as the fractal dimension D extracted from the eigenstates under very general considerations [54]. We note that the behaviour $\Delta_t \sim \mathcal{N}_F^{-(1-D_s)}$ is different from a self-consistent theory [30, 31] of MBL, where the thermodynamic limit of $\mathcal{N}_F \to \infty$ is taken first before taking the $\eta \to 0$ limit. As a result, one obtains $\Delta_t \propto \eta$ and such a theory does not in effect distinguish between Anderson localized and multifractal states.

Further insight into the multifractal behaviour may be gained by analysing the tail of the probability distribution function $P(\Delta)$ of Δ_I over disorder realizations. For finite η and/or \mathcal{N}_F , one expects [54] the distribution to be cut off at a maximum value $\Delta = \Delta_{\max}$, where $\Delta_{\max} \sim 1/\eta_c \sim \mathcal{N}_F^z$ for $\eta \ll \eta_c$. As shown in Fig. 3(a), we indeed find that Δ_{\max} directly extracted from the numerical data follows a power-law $\sim \mathcal{N}_F^z$. The exponent z extracted from Δ_{\max} is shown in Fig. 3(b), and indeed satisfies 0 < z < 1. This further confirms the multifractal scaling of the self-energy in the MBL phase.

Conclusion.— Using a recursive Green function method, we have in summary obtained the critical scaling across the MBL transition by calculating the self-energy associated with the local Fock-space propagator, the typical value of the imaginary part of which, Δ_t , acts as an order parameter for the MBL transition. The finite-size scaling of Δ_t implies the existence of a non-ergodic volume with a KT-like essential singularity, which directly controls the continuous vanishing of Δ_t on approach to the transition from the ergodic side; and the multifractal nature of the MBL phase was demonstrated via determination of the spectral fractal dimension D_s , which was shown to change discontinuously across the transition. While our focus here has been on the local FS propaga-

tor, the recursive Green function method also gives access to the non-local propagator, a question of immediate future interest which can potentially provide insights into the critical scaling of a FS localization length, and also enable study of the inhomogeneous nature of MBL eigenstates on the FS lattice [36]. It would also be interesting to explore further the connection [36] between real-space

and Fock-space critical properties, e.g. how rare thermal regions in real space [55–57] affect the FS self-energy.

SB acknowledges support from SERB (ECR/2018/001742), DST, India. SM acknowledges support from QuST, DST, India. SR acknowledges support from ICTS-Simons Early Career Faculty Fellowship and EPSRC Grant No. EP/S020527/1.

- * equally contributed
- † sjagannath@iisc.ac.in; soumighosh@alum.iisc.ac.in; sthitadhi.roy@icts.res.in; david.logan@chem.ox.ac.uk; smukerjee@iisc.ac.in; sumilan@iisc.ac.in
- [1] Rahul Nandkishore and David A. Huse, "Many-body localization and thermalization in quantum statistical mechanics," Annual Review of Condensed Matter Physics 6, 15–38 (2015).
- [2] Dmitry A. Abanin and Zlatko Papić, "Recent progress in many-body localization," Annalen der Physik 529, 1700169 (2017).
- [3] Fabien Alet and Nicolas Laflorencie, "Many-body localization: An introduction and selected topics," Comptes Rendus Physique 19, 498 525 (2018).
- [4] Dmitry A. Abanin, Ehud Altman, Immanuel Bloch, and Maksym Serbyn, "Colloquium: Many-body localization, thermalization, and entanglement," Rev. Mod. Phys. 91, 021001 (2019).
- [5] J. M. Deutsch, "Quantum statistical mechanics in a closed system," Phys. Rev. A 43, 2046–2049 (1991).
- [6] Mark Srednicki, "Chaos and quantum thermalization," Phys. Rev. E 50, 888–901 (1994).
- [7] Mark Srednicki, "The approach to thermal equilibrium in quantized chaotic systems," Journal of Physics A: Mathematical and General **32**, 1163 (1999).
- [8] D.M. Basko, I.L. Aleiner, and B.L. Altshuler, "Metal-insulator transition in a weakly interacting many-electron system with localized single-particle states," Annals of Physics 321, 1126 – 1205 (2006).
- [9] I. V. Gornyi, A. D. Mirlin, and D. G. Polyakov, "Interacting electrons in disordered wires: Anderson localization and low-t transport," Phys. Rev. Lett. 95, 206603 (2005)
- [10] John Z. Imbrie, "On many-body localization for quantum spin chains," Journal of Statistical Physics 163, 998–1048 (2016).
- [11] Vadim Oganesyan and David A. Huse, "Localization of interacting fermions at high temperature," Phys. Rev. B 75, 155111 (2007).
- [12] Marko Žnidarič, T. Prosen, and Peter Prelovšek, "Manybody localization in the Heisenberg XXZ magnet in a random field," Phys. Rev. B 77, 064426 (2008).
- [13] Arijeet Pal and David A. Huse, "Many-body localization phase transition," Phys. Rev. B 82, 174411 (2010).
- [14] Jens H. Bardarson, Frank Pollmann, and Joel E. Moore, "Unbounded growth of entanglement in models of manybody localization," Phys. Rev. Lett. 109, 017202 (2012).
- [15] Jonas A. Kjäll, Jens H. Bardarson, and Frank Pollmann, "Many-body localization in a disordered quantum Ising chain," Phys. Rev. Lett. 113, 107204 (2014).
- [16] Maksym Serbyn, Z. Papić, and Dmitry A. Abanin, "Criterion for many-body localization-delocalization phase

- transition," Phys. Rev. X 5, 041047 (2015).
- [17] David J. Luitz, Nicolas Laflorencie, and Fabien Alet, "Many-body localization edge in the random-field heisenberg chain," Phys. Rev. B 91, 081103 (2015).
- [18] Philipp T. Dumitrescu, Anna Goremykina, Siddharth A. Parameswaran, Maksym Serbyn, and Romain Vasseur, "Kosterlitz-thouless scaling at many-body localization phase transitions," Phys. Rev. B 99, 094205 (2019).
- [19] Maximilian Kiefer-Emmanouilidis, Razmik Unanyan, Michael Fleischhauer, and Jesko Sirker, "Evidence for unbounded growth of the number entropy in many-body localized phases," Phys. Rev. Lett. **124**, 243601 (2020).
- [20] Jan Šuntajs, Janez Bonča, Toma ž Prosen, and Lev Vidmar, "Quantum chaos challenges many-body localization." Phys. Rev. E 102, 062144 (2020).
- [21] Rajat K Panda, Antonello Scardicchio, Maximilian Schulz, Scott R Taylor, and Marko Žnidarič, "Can we study the many-body localisation transition?" EPL (Europhysics Letters) 128, 67003 (2020).
- [22] Jan Šuntajs, Janez Bonča, Toma ž Prosen, and Lev Vidmar, "Quantum chaos challenges many-body localization," Phys. Rev. E 102, 062144 (2020).
- [23] D.A. Abanin, J.H. Bardarson, G. De Tomasi, S. Gopalakrishnan, V. Khemani, S.A. Parameswaran, F. Pollmann, A.C. Potter, M. Serbyn, and R. Vasseur, "Distinguishing localization from chaos: Challenges in finite-size systems," Annals of Physics 427, 168415 (2021).
- [24] Ranjan Modak and Subroto Mukerjee, "Many-body localization in the presence of a single-particle mobility edge," Phys. Rev. Lett. 115, 230401 (2015).
- [25] Vedika Khemani, D. N. Sheng, and David A. Huse, "Two universality classes for the many-body localization transition," Phys. Rev. Lett. 119, 075702 (2017).
- [26] Anna Goremykina, Romain Vasseur, and Maksym Serbyn, "Analytically solvable renormalization group for the many-body localization transition," Phys. Rev. Lett. 122, 040601 (2019).
- [27] Alan Morningstar and David A. Huse, "Renormalization-group study of the many-body localization transition in one dimension," Phys. Rev. B 99, 224205 (2019).
- [28] Alan Morningstar, David A. Huse, and John Z. Imbrie, "Many-body localization near the critical point," Phys. Rev. B 102, 125134 (2020).
- [29] Boris L. Altshuler, Yuval Gefen, Alex Kamenev, and Leonid S. Levitov, "Quasiparticle lifetime in a finite system: A nonperturbative approach," Phys. Rev. Lett. 78, 2803–2806 (1997).
- [30] David E. Logan and Staszek Welsh, "Many-body localization in Fock space: A local perspective," Phys. Rev. B 99, 045131 (2019).
- [31] Sthitadhi Roy and David E. Logan, "Fock-space correla-

- tions and the origins of many-body localization," Phys. Rev. B **101**, 134202 (2020).
- [32] Alexander Altland and Tobias Micklitz, "Field theory approach to many-body localization," Phys. Rev. Lett. 118, 127202 (2017).
- [33] Soumi Ghosh, Atithi Acharya, Subhayan Sahu, and Subroto Mukerjee, "Many-body localization due to correlated disorder in Fock space," Phys. Rev. B 99, 165131 (2019).
- [34] A. De Luca and A. Scardicchio, "Ergodicity breaking in a model showing many-body localization," EPL (Europhysics Letters) 101, 37003 (2013).
- [35] Nicolas Macé, Fabien Alet, and Nicolas Laflorencie, "Multifractal scalings across the many-body localization transition," Phys. Rev. Lett. 123, 180601 (2019).
- [36] Sthitadhi Roy and David E. Logan, "Fock-space anatomy of eigenstates across the many-body localization transition," Phys. Rev. B 104, 174201 (2021).
- [37] Giuseppe De Tomasi, Ivan M. Khaymovich, Frank Poll-mann, and Simone Warzel, "Rare thermal bubbles at the many-body localization transition from the fock space point of view," Phys. Rev. B 104, 024202 (2021).
- [38] Eugene Feenberg, "A note on perturbation theory," Phys. Rev. **74**, 206–208 (1948).
- [39] E. N. Economou, Green's Functions in Quantum Physics (Springer, Berlin, 2006).
- [40] P. W. Anderson, "Absence of diffusion in certain random lattices," Phys. Rev. 109, 1492–1505 (1958).
- [41] R. Abou-Chacra, D. J. Thouless, and P. W. Anderson, "A selfconsistent theory of localization," Journal of Physics C Solid State Physics 6, 1734–1752 (1973).
- [42] E. N. Economou and Morrel H. Cohen, "Existence of mobility edges in anderson's model for random lattices," Phys. Rev. B 5, 2931–2948 (1972).
- [43] D. C. Licciardello and E. N. Economou, "Study of localization in anderson's model for random lattices," Phys. Rev. B 11, 3697–3717 (1975).
- [44] Francesca Pietracaprina, Nicolas Macé, David J. Luitz, and Fabien Alet, "Shift-invert diagonalization of large many-body localizing spin chains," SciPost Phys. 5, 45 (2018).
- [45] Piotr Sierant, Maciej Lewenstein, and Jakub Zakrzewski, "Polynomially filtered exact diagonalization approach to many-body localization," Phys. Rev. Lett. 125, 156601 (2020).
- [46] Patrick A. Lee and Daniel S. Fisher, "Anderson localization in two dimensions," Phys. Rev. Lett. 47, 882–885 (1981).
- [47] A MacKinnon, "The conductivity of the one-dimensional disordered Anderson model: a new numerical method," Journal of Physics C: Solid State Physics 13, L1031– L1034 (1980).
- [48] A. MacKinnon and B. Kramer, "The scaling theory of electrons in disordered solids: Additional numerical results," Zeitschrift für Physik B Condensed Matter **53**, 1–13 (1983).
- [49] I. García-Mata, O. Giraud, B. Georgeot, J. Martin, R. Dubertrand, and G. Lemarié, "Scaling theory of the anderson transition in random graphs: Ergodicity and universality," Phys. Rev. Lett. 118, 166801 (2017).
- [50] Nicolas Laflorencie, Gabriel Lemarié, and Nicolas Macé, "Chain breaking and kosterlitz-thouless scaling at the many-body localization transition in the random-field heisenberg spin chain," Phys. Rev. Research 2, 042033

- (2020).
- [51] Bela Bauer and Chetan Nayak, "Area laws in a manybody localized state and its implications for topological order," Journal of Statistical Mechanics: Theory and Experiment 2013, P09005 (2013).
- [52] Staszek Welsh and David E Logan, "Simple probability distributions on a fock-space lattice," Journal of Physics: Condensed Matter 30, 405601 (2018).
- [53] J. A. Verges, "Computational implementation of the Kubo formula for the static conductance: application to two-dimensional quantum dots," Computer Physics Communications 118, 71–80 (1999).
- [54] B. L. Altshuler, L. B. Ioffe, and V. E. Kravtsov, "Multifractal states in self-consistent theory of localization: analytical solution," (2016), arXiv:1610.00758 [cond-mat.dis-nn].
- [55] Wojciech De Roeck and Fran çois Huveneers, "Stability and instability towards delocalization in many-body localization systems," Phys. Rev. B 95, 155129 (2017).
- [56] David J. Luitz, Fran çois Huveneers, and Wojciech De Roeck, "How a small quantum bath can thermalize long localized chains," Phys. Rev. Lett. 119, 150602 (2017).
- [57] Ionut-Dragos Potirniche, Sumilan Banerjee, and Ehud Altman, "Exploration of the stability of many-body localization in d > 1," Phys. Rev. B **99**, 205149 (2019).

Supplemental Material

for

Scaling of Fock-space propagator and multifractality across the many-body localization transition by Jagannath Sutradhar^{1,*}, Soumi Ghosh^{1,2,*}, Sthitadhi Roy^{2,3,4}, David E. Logan^{3,5}, Subroto Mukerjee¹, Sumilan Banerjee¹

S1: Recursive Green function Method

In the recursive method, we calculate different elements of the Green function by starting from one of the two minimally connected Fock-space sites ($|111...000\rangle$, $|000...111\rangle$) and by adding the next slice connected by hopping to the earlier slice at each step. Here we start with the top site $|111...000\rangle$ as shown in Fig. 1(a). At each iteration step, the method inverts a matrix containing the Hamiltonian elements for the added slice and is, therefore, of size $\mathcal{N}_{\ell} \times \mathcal{N}_{\ell}$, where \mathcal{N}_{ℓ} is the size of the added slice. Hence, this method avoids the inversion of the full Hamiltonian in Eq. (2). The maximum size of the matrix $(\mathcal{N}_{M} \times \mathcal{N}_{M})$ that is inverted during the calculation is determined by the number of sites \mathcal{N}_{M} in the middle slice, which is the largest slice of the Fock space [Fig. 1(a)]. For L between 10 and 22, \mathcal{N}_{M} is between $\sim 1-2$ orders of magnitude lower than the full Fock-space dimension $\mathcal{N}_{F} = \binom{L}{L/2}$. It is this substantial reduction that provides the advantage to achieve the system size L=22 even with serial computation. The method can be applied to even larger systems like L=24 with parallelization.

At the ℓ -th step of recursion, let $H^{(\ell)}$ be the Hamiltonian corresponding to the part of the Fock space lattice containing all slices up to the ℓ -th slice. The corresponding Green function for these ℓ slices is given by $G^{(\ell)} = \left[(E + i\eta)\mathbb{1} - H^{(\ell)} \right]^{-1}$. Using Eq. (2) and the local structure of the Fock space lattice, the Hamiltonian corresponding to all slices up to the $(\ell + 1)$ -th slice can be written as:

$$H^{(\ell+1)} = \begin{pmatrix} H^{(\ell)} & \mathcal{T}_{lr} \\ T_{rl} & H^{(0)(\ell+1)} \end{pmatrix}$$

$$H^{(0)(\ell+1)} = \sum_{s,s' \in (\ell+1)} T_{s,s'} |s, \ell+1\rangle \langle s', \ell+1| + \sum_{s \in (\ell+1)} \mathcal{E}_{s,\ell+1} |s, \ell+1\rangle \langle s, \ell+1|$$

$$\mathcal{T}_{lr} = \sum_{s \in \ell} \sum_{s' \in (\ell+1)} T_{s,s'} |s', \ell+1\rangle \langle s, \ell|$$

where $H^{(0)(\ell+1)}$ contains the part of the Hamiltonian corresponding to the $(\ell+1)$ -th slice disconnected from the rest of the Fock lattice, \mathcal{T}_{lr} contains the hopping elements for hopping from the ℓ -th slice to the $(\ell+1)$ -th slice and $\mathcal{T}_{rl} = \mathcal{T}_{lr}^{\dagger}$. Similarly, the Green function at the $(\ell+1)$ -th step can be written as

$$G^{(\ell+1)} = \begin{pmatrix} G_l^{(\ell+1)} & G_{lr}^{(\ell+1)} \\ G_{rl}^{(\ell+1)} & G_r^{(\ell+1)} \end{pmatrix}.$$

Here the subscript l denotes the matrix elements of the left part (first to the ℓ -th slice), and r denotes the elements of the $(\ell+1)$ -th slice, as described in Fig. S1. Then, at the $(\ell+1)$ -th step of recursion, the Green function $G^{(\ell+1)}$ and the Hamiltonian $H^{(\ell+1)}$ have the following matrix equation.

$$\begin{bmatrix} E^{+} \mathbb{1} - H^{(\ell+1)} \end{bmatrix} G^{(\ell+1)} = \mathbb{1}$$

$$\Rightarrow \begin{pmatrix} (G^{(\ell)})^{-1} & \mathcal{T}_{lr} \\ \mathcal{T}_{rl} & (G^{0(\ell+1)})^{-1} \end{pmatrix} \begin{pmatrix} G_{l}^{(\ell+1)} & G_{lr}^{(\ell+1)} \\ G_{rl}^{(\ell+1)} & G_{r}^{(\ell+1)} \end{pmatrix} = \mathbb{1}.$$
(S1.1)

Here $(G^{(\ell)})^{-1} = (E^+\mathbb{1} - H^{(\ell)})$ and $(G^{0(\ell+1)})^{-1}$ is given by $[E^+\mathbb{1} - H^{(0)(\ell+1)}]$. From the above equation, we can obtain the following equation

$$\begin{split} G_l^{(\ell+1)} &= G^{(\ell)} + G^{(\ell)} \mathcal{T}_{lr} G_{rl}^{(\ell+1)}, \\ \langle s|G_l^{(\ell+1)}|s'\rangle &= \langle s|G^{(\ell)}|s'\rangle + \langle s|G^{(\ell)}\left(\mathbb{T}_{\ell}\left|\ell\right\rangle\left\langle\ell+1\right|\right) \, G_{rl}^{(\ell+1)}|s'\rangle \,, \qquad s,s' \leq \ell. \end{split}$$

Note that $\langle s|A|s'\rangle = A(s,s')$ denotes an element of a rectangular matrix A, as each of the slices, indexed by s and s', contains different numbers of lattice points in general. For the same reason, \mathbb{T}_{ℓ} is also a rectangular matrix containing hopping matrix elements between ℓ -th and $(\ell+1)$ -th slices. Therefore,

$$G^{(\ell+1)}(s,s') = G^{(\ell)}(s,s') + G^{(\ell)}(s,\ell) \mathbb{T}_{\ell} G^{(\ell+1)}(\ell+1,s'), \quad \ s,s' \leq \ell.$$

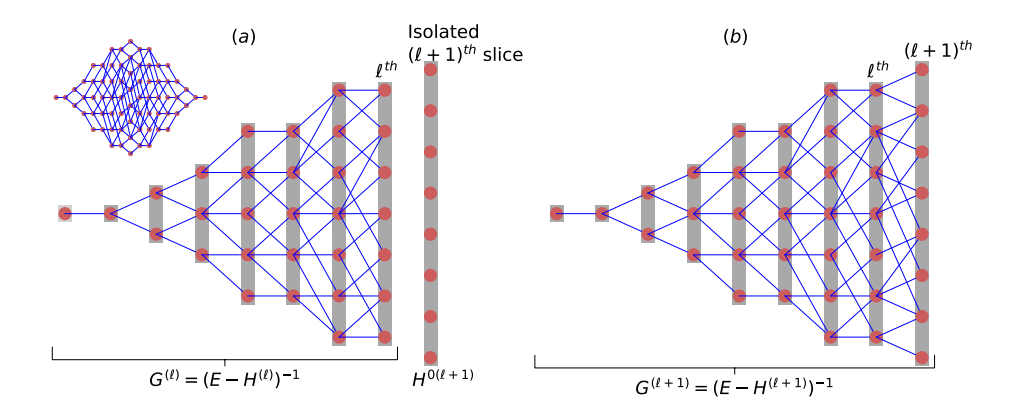


FIG. S1. (a) The figure on the top left corner is similar to Fig. 1(a), but rotated by 90° . The larger figure shows a part of it, up to ℓ th slice, where the grey shaded area shows each slice. Orange circles and solid blue lines represent the FS sites and hopping, respectively. (b) As we keep on adding the next slices, the Green function of the left part gets updated via the iterative Eqs. (S1.2).

Similarly, starting from Eq. (S1.1),

$$G^{(\ell+1)}(\ell+1,s) = G^{(\ell+1)}(\ell+1,\ell+1)\mathbb{T}_{\ell}^{\dagger}G^{(\ell)}(\ell,s) \quad s \le \ell,$$
(S1.2a)

$$G^{(\ell+1)}(s,\ell+1) = G^{(\ell)}(s,\ell) \mathbb{T}_{\ell}^{\dagger} G^{(\ell+1)}(\ell+1,\ell+1) \quad s \le \ell.$$
 (S1.2b)

Therefore,

$$G^{(\ell+1)}(s,s') = G^{(\ell)}(s,s') + G^{(\ell)}(s,\ell) \mathbb{T}_{\ell} G^{(\ell+1)}(\ell+1,\ell+1) \mathbb{T}_{\ell} G^{(\ell)}(\ell,s') \quad s,s' \leq \ell,$$
 (S1.2c)

and on-slice elements

$$G^{(\ell+1)}(\ell+1,\ell+1) = \left[\left(G^{0(\ell+1)} \right)^{-1} - \underbrace{\mathbb{T}_{\ell}^{\dagger} G^{(\ell)}(\ell,\ell) \mathbb{T}_{\ell}}_{\text{self energy } \Sigma^{(\ell)}} \right]^{-1}. \tag{S1.2d}$$

Using Eqs. (S1.2), we can calculate the desired elements of the Green function, avoiding the inversion of a matrix having the dimension of the full Fock space.

In Table I, we show the number of disorder configurations considered for different sizes to generate the distributions of diagonal and off-diagonal elements of the Green function. We have verified that the distributions do not change further with an increasing number of disorder configurations.

TABLE I. L and corresponding number of disorder configurations considered to generate the distributions of Δ_I at each W point.

L	# disorder realization
12	10,000
14	5,000
16	2,000
18	1,000
20	500
22	130

S2: Distribution of Feenberg self-energy

For both the ergodic and MBL phases, Fig. S2 gives a representative example of the fact that the distributions of the imaginary part of the self-energy $(P(\Delta_I) \text{ or } P(\Delta_I/\eta))$ are barely affected whether one considers $I \in M$ or $I \in \text{all}$ Fock-space sites.

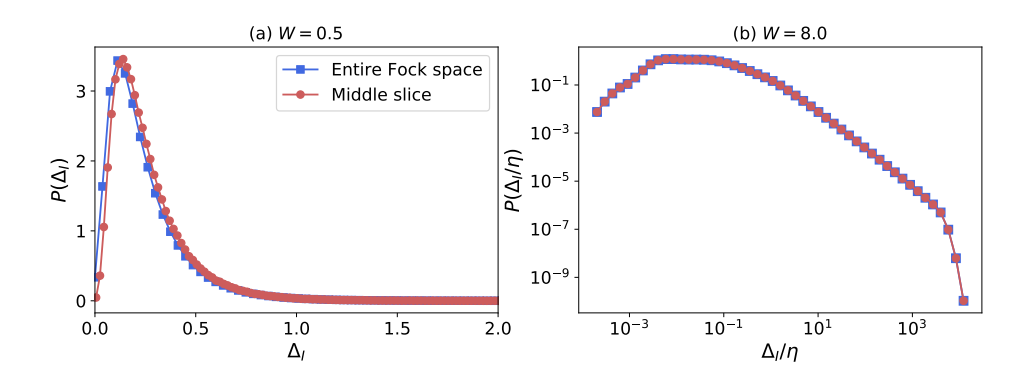


FIG. S2. The probability distributions of the imaginary part Δ_I of the self-energy, considering both $I \in M$ and $I \in FS$. These match well with each other, in both the thermal phase (shown in (a)) and MBL phase ((b)). Data shown in the figure is for system size L = 14.

S3: Scaling of Δ_t

Asymptotic behaviour of the scaling functions:

In the ergodic phase, the scaling ansatz Eq. (3) reads

$$\ln \Delta_t = \ln \Delta_c + \mathcal{F}_{\text{vol}}(\mathcal{N}_F/\Lambda)$$

with the critical $\Delta_c = C_c \mathcal{N}_F^{-(1-D_c)}$ and C_c a constant; equivalently,

$$\mathcal{F}_{\text{vol}}\left(\frac{\mathcal{N}_F}{\Lambda}\right) = \ln \Delta_t - \ln C_c + (1 - D_c) \ln \Lambda + (1 - D_c) \ln \frac{\mathcal{N}_F}{\Lambda}.$$
 (S3.1)

Deep in an ergodic phase, both Λ and Δ_t are $\mathcal{O}(1)$. From Eq. (S3.1), for $x = \mathcal{N}_F/\Lambda \gg 1$ the asymptotic large-x behaviour of $\mathcal{F}_{\text{vol}}(x)$ is then

$$\mathcal{F}_{\text{vol}}(x) \sim (1 - D_c) \ln x \tag{S3.2}$$

up to $\mathcal{O}(1)$ corrections. Its slope gives the fractal exponent $(1 - D_c)$ for $W = W_c$, which is also found to be consistent with the numerical asymptotic fit in Fig. 1(b).

On the other hand, in the MBL phase $W > W_c$, $\Delta_t = C_m \mathcal{N}_F^{-(1-D_s)}$ (Fig. 1(b)), where C_m and D_s both depend on W. The scaling ansatz Eq. (3) then gives

$$\mathcal{F}_{\text{lin}}\left(\frac{\ln \mathcal{N}_F}{\xi}\right) = \ln \frac{C_m}{C_c} - (1 - D_c) \frac{\ln \mathcal{N}_F}{\xi},\tag{S3.3}$$

with ξ defined as

$$\xi = \frac{(1 - D_c)}{D_c - D_s}. ag{S3.4}$$

As $D_s \to D_c^+$, i.e. as $W \to W_c^+$, we see that ξ diverges. Deep in the MBL phase, where $x = (\ln N_F)/\xi \gg 1$, the asymptotic scaling is clearly

$$\mathcal{F}_{\text{lin}}(x) \sim -(1 - D_c)x. \tag{S3.5}$$

Finally, returning to the ergodic phase, Eq. (S3.1) with $x = \mathcal{N}_F/\Lambda$ can be cast as

$$\Delta_t = \Lambda^{-(1-D_c)} \exp \left[\mathcal{F}_{\text{vol}}(x) - (1 - D_c) \ln x + \ln C_c \right]$$
 (S3.6)

where (as shown in the main text) the non-ergodic volume $\Lambda \sim \exp[b/\sqrt{W_c - W}]$ is determined by W, and C_c is a constant. For any $W < W_c$, and hence for any finite Λ no matter how large, the thermodynamic limit corresponds to

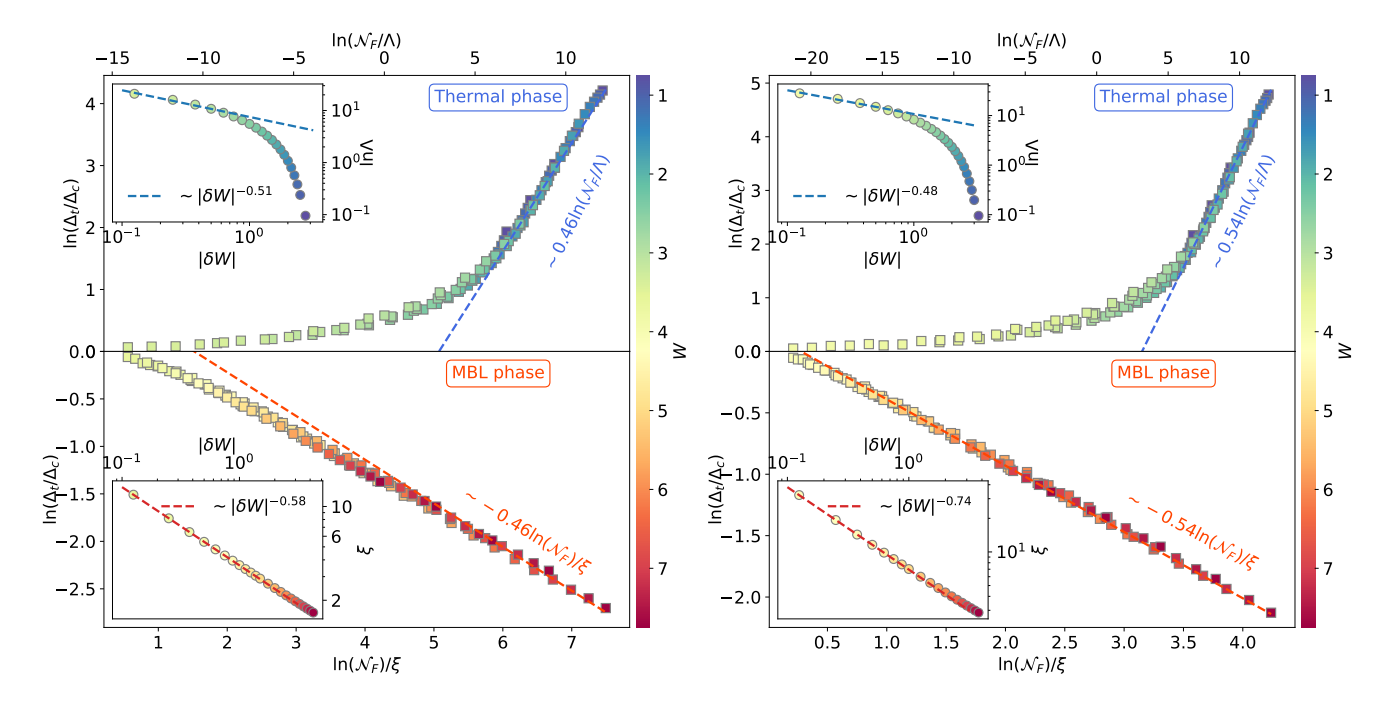


FIG. S3. Finite-size scaling collapse of $\ln(\Delta_t/\Delta_c)$ in direct parallel to that of Fig. 2 for $W_c=3.75$, but here shown for $W_c=3.5$ (left panel) and $W_c=4.0$ (right panel).

 $x \to \infty$. From Eq. (S3.2) the argument of the exponential in Eq. (S3.6) is then $\mathcal{O}(1)$, so in the thermodynamic limit the order parameter Δ_t vanishes continuously as

$$\Delta_t \sim \Lambda^{-(1-D_c)}$$
 (S3.7)

and is controlled by Λ .

Dependence of scaling results on W_c :

For the finite-size scaling shown in Fig. 2, $W_c = 3.75$ was employed. Fig. S3 gives corresponding results for the scaling collapse on choosing $W_c = 3.5$ and 4. As seen, the quality of scaling is quite robust to the variation in W_c .